



Numerical Simulation of Spectral and Timing Properties of a Two Component Advective Flow around a Black Hole

S. K. Garain^{1*}, H. Ghosh² and S. K. Chakrabarti^{1,2}

¹*S N Bose National Centre for Basic Sciences, Block JD, Sector III, Salt Lake, Kolkata 700098, India*

²*Indian Centre for Space Physics, Chalantika 43, Garia Station Road, Garia, Kolkata 700084, India*

Received — ; accepted —

Abstract. We study the spectral and timing properties of a two component advective flow (TCAF) around a black hole by numerical simulation. Several cases have been simulated by varying the Keplerian disk rate and the resulting spectra and lightcurves have been produced for all the cases. The dependence of the spectral states and quasi-periodic oscillation (QPO) frequencies on the flow parameters is discussed. We also find the earlier explanation of arising of QPOs as the resonance between infall time scale and cooling time scale remain valid even for Compton cooling.

Keywords : accretion, accretion discs; black hole physics; hydrodynamics; radiative transfer; shock waves; methods: numerical

1. Introduction

The spectral and timing properties of the accretion disk around a black hole give away the vital information about understanding the nature of the black hole at the centre. Assuming the most general accretion flow configuration, namely, two-component advective flow (TCAF) model (Chakrabarti & Titarchuk 1995), we study by numerical simulation how the spectral and timing properties of an accretion disk around a black hole are explained.

*email: sudip@bose.res.in

2. Simulation Set Up and Procedure

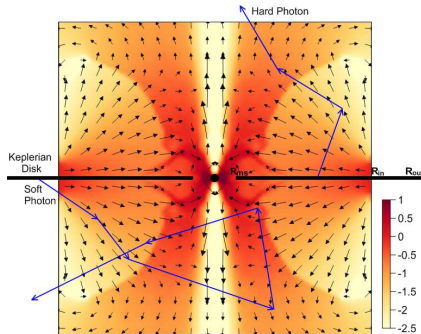


Figure 1. The schematic diagram of our simulation set up. The velocity vectors of the infalling matter are shown. The colors show the normalized density in a logarithmic scale. The zig-zag trajectories (blue online) are the typical path followed by the photons. The velocity vectors are plotted for $\lambda = 1.73$ and $\epsilon = 0.0021$.

In Figure 1, the schematic diagram of our simulation set up is presented. The outer boundary of the sub-Keplerian matter is at $R_{in} = 100r_g$ ($r_g = \frac{2GM}{c^2}$) whereas that of the Keplerian disk at the equatorial plane is located at $R_{out} = 200r_g$. At the center, a non-rotating black hole of mass $10M_{\odot}$ is located. The sub-Keplerian flow dynamics is simulated using a TVD code (Molteni, Ryu & Chakrabarti 1996; Giri, Chakrabarti, Samanta & Ryu 2010). For a particular simulation, we use the Keplerian disk rate (\dot{m}_d) and the sub-Keplerian halo rate (\dot{m}_h) as parameters. The specific energy (ϵ) and the specific angular momentum (λ) determines the hydrodynamics (shock location, number density and velocity variations etc.) and the thermal properties of the sub-Keplerian matter. The radiative properties of the accretion disk is studied using a Monte Carlo code (Poznyakov, Sobol & Sunyaev 1983; Ghosh, Chakrabarti & Laurent 2009). The hydrodynamic code and the radiative transfer code are coupled together and are run back to back. The details of the coupling procedure can be found in Ghosh, Garain, Giri & Chakrabarti (2011) and Garain, Ghosh & Chakrabarti (2012).

3. Results and Discussions

Case ID	ϵ, λ	\dot{m}_d	\dot{m}_h	$\langle R_{sh} \rangle$	v_{QPO}	$\langle \alpha \rangle$	$\frac{t_{in}}{t_{cool}}$
C1	0.0021, 1.73	1E-4	0.1	25.75	No QPO	0.826	0.694
C2	0.0021, 1.73	2E-4	0.1	22.82	10.63	0.853	0.844
C3	0.0021, 1.73	3E-4	0.1	20.39	12.34	0.868	0.954
C4	0.0021, 1.73	4E-4	0.1	18.62	14.63	0.873	0.944
C5	0.0021, 1.73	5E-4	0.1	18.33	22.74	0.901	1.071
C6	0.0021, 1.73	1E-3	0.1	15.02	18.2	1.074	0.993
C7	0.0021, 1.73	1E-2	0.1	3.4	No QPO	1.139	3.558
C8	0.0021, 1.73	1E-1	0.1	3.6	No QPO	1.102	33.236

In Table 1, we show the parameters used for the simulations and a summary

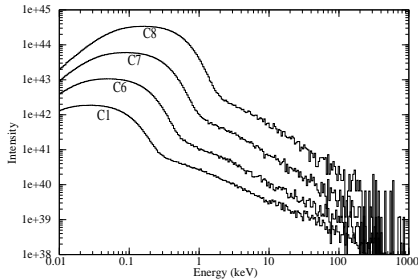


Figure 2. Variation of the shape of the spectrum when \dot{m}_d is increased by a factor of 10 starting from $\dot{m}_d = 0.0001$ to 0.1 keeping halo rate constant at $\dot{m}_h = 0.1$. Case IDs are marked for each plot. The spectrum becomes softer as \dot{m}_d is increased.

of the results. In column 5, we present the time averaged shock location in r_g near the equatorial plane. For some combinations of \dot{m}_d and \dot{m}_h , we find QPOs and we list the QPO frequencies (Hz) in column 6. The time averaged spectral slope (α , $I(E) \propto E^{-\alpha}$) is given in column 7. In the last column, we show the ratio of the infall time scale (t_{in}) and the cooling time scale (t_{cool}).

Spectral properties:

In Figure 2, we show the variations of the shape of the final emergent spectra. The case IDs are marked on each plot. As \dot{m}_d is increased, the relative intensity increases since increasing \dot{m}_d increases the number of soft photons in a given energy band. However, the spectra become softer as the centrifugal pressure dominated inner region (including the post-shock region, when present) is cooled faster and the region collapses with the increase of \dot{m}_d . Also, the number of available hot electrons reduces.

Timing properties:

We compute the time variations of the photon count rates for all the cases in order to generate simulated lightcurves. In Figure 3a, we plot lightcurves of the photons in the energy band 0.5keV to 100keV (for C7 and C8, $2 \text{ keV} < E < 100 \text{ keV}$). The photons in this energy range are mostly the inverse-Comptonized photons. The variations in the lightcurves are arising because of the variations in the hydrodynamic and thermal properties of the post-shock region. In Figure 3b, we show the Power Density Spectra (PDS) for all the cases. We find low frequency quasi-periodic oscillations (LFQPO) for some cases. The frequencies are listed in Table 1. We find that LFQPO frequencies increase with the increase of \dot{m}_d . We have seen that the spectra become softer with the increase of \dot{m}_d . Therefore from Figures 2 and 3b, we find that the LFQPO increases as the object transits from the harder state to the softer states.

It has been argued in literature (Molteni, Sponholz & Chakrabarti 1996; Chakrabarti, Acharyya & Molteni 2004) that the oscillation in the centrifugal barrier dominated hot region is responsible for the LFQPO observed in the black hole candidates. LFQPO arises when the infall time scale of post-shock matter roughly matches with the cooling time scale. For the present case, we

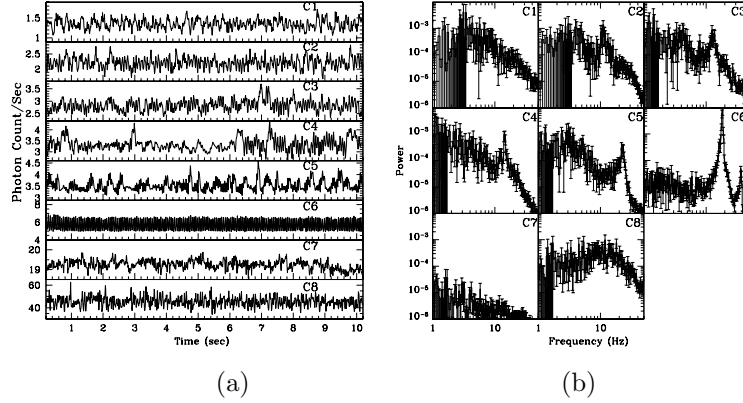


Figure 3. a) The lightcurves of the photons (in the unit of 10^{42}) which are in the power-law region ($0.5\text{keV} < E < 100\text{keV}$) and b) the Power Density Spectra (PDS) for these cases are presented. Here, \dot{m}_d is increased keeping $\dot{m}_h = 0.1$ constant.

compute the infall time scale t_{in} and the cooling time scale t_{cool} , and we present the ratio $\frac{t_{in}}{t_{cool}}$ in the last column of Table 1. We see that this ratio is nearly 1 for all the cases when LFQPOs are seen. Thus the proposal of LFQPOs arising out of resonance oscillation of the post-shock region appears to be justified.

Acknowledgements

The work of HG was supported by a post doctoral grant from Ministry of Earth Science, Government of India. The authors acknowledge the organizers for providing the local hospitality at Indian Institute of Technology, Guwahati, India during the conference.

References

- Chakrabarti S. K., Titarchuk L.G. 1995, ApJ 455, 623
Molteni D., Ryu D., Chakrabarti S. K., 1996, ApJ, 470, 460
Giri K., Chakrabarti S. K., Samanta M. M., Ryu D., 2010, MNRAS, 403, 516
Poznyakov, L., Sobol, I., Sunyaev, R., 1983, A & Sp Physics Reviews 2, 189
Ghosh H., Chakrabarti S. K., Laurent P., 2009, IJMPD, 18, 1693
Ghosh H., Garain S. K., Giri K., Chakrabarti S. K., 2011, MNRAS, 416, 959
Garain S. K., Ghosh H., Chakrabarti S. K., 2012, ApJ, 758, 114
Molteni D., Sponholz H., Chakrabarti S. K., 1996, ApJ, 457, 805
Chakrabarti S. K., Acharyya K., Molteni, D., 2004, A&A, 21, 1